The Meteoritical Society

Meteoritics & Planetary Science 50, Nr 8, 1392–1407 (2015)
doi: 10.1111/maps.12475

Iron isotopic measurements in presolar silicate and oxide grains from the Acfer 094 ungrouped carbonaceous chondrite

Wei Jia ONG[1,2] and Christine FLOSS[1*]

[1]Laboratory for Space Sciences and Physics Department, Washington University, One Brookings Drive, St. Louis, Missouri 63130, USA
[2]National Superconducting Cyclotron Laboratory, Michigan State University, 640 S. Shaw Lane, East Lansing, Michigan 48824, USA
*Corresponding author. E-mail: floss@wustl.edu

(Received 21 November 2014; revision accepted 05 May 2015)

Abstract–We carried out Fe isotopic analyses on 21 O-rich presolar grains from the Acfer 094 ungrouped carbonaceous chondrite. Presolar grains were identified on the basis of oxygen isotopic ratios, and elemental compositions were measured by Auger spectroscopy. The Fe isotopic measurements were carried out by analyzing the Fe isotopes as negative secondary oxides with the NanoSIMS to take advantage of the higher spatial resolution of the Cs^+ primary ion beam. Our results demonstrate the effectiveness of this approach for measuring both $^{54}Fe/^{56}Fe$ and $^{57}Fe/^{56}Fe$. The ion yield for FeO^- is significantly lower than for Fe^+, but this is not a serious limitation for presolar silicate grains with Fe as a major element. Most of the grains analyzed are ferromagnesian silicates, but we also measured four oxide grains. Iron contents are high in all of the grains, ranging from 10 to 40 atom%. Three of the grains belong to oxygen isotope Group 4. All of them have $^{54}Fe/^{56}Fe$ and $^{57}Fe/^{56}Fe$ ratios that are solar within errors, consistent with an origin in the outer zones of a Type II supernova, as indicated by their oxygen isotopic compositions. The remaining grains belong to oxygen isotope Group 1, with origins in low-mass AGB stars. The majority of these also have solar $^{54}Fe/^{56}Fe$ and $^{57}Fe/^{56}Fe$ ratios. However, four grains are depleted in ^{57}Fe; one is also slightly depleted in ^{54}Fe. Current AGB models predict excesses in ^{57}Fe with $^{54}Fe/^{56}Fe$ ratios that largely reflect the metallicity of the parent star. While the solar $^{57}Fe/^{56}Fe$ ratios are consistent with formation of the grains in early third dredge-up episodes, these models cannot account for the grains with ^{57}Fe depletions. Comparison with galactic evolution models suggests formation of these grains from stars with significantly subsolar metallicity; however, these models also predict large depletions in ^{54}Fe, which are not observed in the grains. Thus, the isotopic compositions of these grains remain unexplained.

INTRODUCTION

Stardust is a small, but ubiquitous, component of certain primitive extraterrestrial materials (e.g., Zinner 2013). These grains formed in the stellar outflows of red giant branch (RGB) and asymptotic giant branch (AGB) stars, or in the ejecta of supernovae, and were subsequently incorporated into the molecular cloud from which the Sun and our solar system formed 4.6 Gyr ago. They can be found today in meteorites, interplanetary dust particles (IDPs), and other samples that largely escaped nebular and planetary processing during and after their formation. Presolar stardust grains give us information about grain formation in stellar environments, providing an astrophysical "snapshot" of the stars from which they originated. They also provide us with "ground truth" data that can be used to inform and constrain models of stellar evolution and nucleosynthesis.

Presolar silicate grains are among the most abundant of the different types of stardust identified in extraterrestrial samples, and they provide unique

opportunities to understand grain formation and nucleosynthesis in O-rich evolved stars. However, they also present unique analytical challenges. Unlike refractory, C-rich presolar phases such as SiC, graphite, and diamond, which can be isolated from their host meteorites by extensive acid treatment (e.g., Amari et al. 1994), presolar silicates cannot be extracted through such chemical procedures, and must be identified through in situ imaging techniques, either in standard meteorite thin sections or in physically disaggregated grain size separates. The identification and analysis of presolar silicate grains is further complicated by the fact that these small grains (typically ~300 nm) are surrounded by isotopically normal solar system silicates, leading to contamination and signal dilution problems (e.g., Nguyen et al. 2007). Despite these limitations, studies of presolar silicate grains over the last 10 yr have provided a wealth of information about their isotopic and elemental compositions (e.g., Messenger et al. 2003, 2005; Nguyen and Zinner 2004; Nguyen et al. 2007, 2010; Floss and Stadermann 2009, 2012; Vollmer et al. 2009; Bose et al. 2010, 2012; Nguyen and Messenger 2014).

Presolar grains provide information about fundamental astrophysical processes such as stellar nucleosynthesis and galactic chemical evolution. Iron is of particular interest in this regard, because of its importance in *s*-process nucleosynthesis. However, the data obtained to date, which largely come from presolar SiC, indicate that the Fe isotopic compositions of some grains are not easily explained by current stellar models. Specifically, some mainstream SiC grains of AGB origin exhibit deficits in ^{57}Fe that are not predicted from AGB nucleosynthesis models (Marhas et al. 2008). Similarly, some SiC and oxide grains from supernovae that are depleted in ^{54}Fe and ^{57}Fe (Floss et al. 2008; Marhas et al. 2008) are not easily understood in terms of current supernova models. Presolar silicate grains are good candidates for Fe isotopic measurements because most have high Fe contents (Floss and Stadermann 2009; Vollmer et al. 2009; Bose et al. 2010; Nguyen et al. 2010). Secondary alteration processes can enhance Fe contents in some presolar silicates (e.g., Floss and Stadermann 2012), but the pristine nature of most of the primitive meteorites in which these grains are found suggests that much of the Fe is intrinsic to the grains. Thus, Fe isotopic measurements of presolar silicates have the potential to provide constraints on stellar nucleosynthesis models. Here, we report on NanoSIMS measurements of the Fe isotopes in presolar silicate grains from the ungrouped carbonaceous chondrite Acfer 094, and compare the results to literature data and current models of stellar nucleosynthesis. Preliminary results have been reported by Ong et al. (2012), Floss et al. (2012), and Ong and Floss (2013).

EXPERIMENTAL

Acfer 094 is the first meteorite in which presolar silicate grains were identified (Nagashima et al. 2004; Nguyen and Zinner 2004), and subsequent studies have shown that these grains are present in high abundance (~160 ppm; Vollmer et al. 2009) in the matrix of this chondrite. For this study, we used a physically disaggregated grain size separate of Acfer 094 matrix material prepared by Nguyen (2005). Samples from the 0.1–0.5 μm fraction were deposited on high purity gold foil for NanoSIMS analysis.

Isotopically anomalous grains were initially identified through C and O raster ion imaging using the Washington University NanoSIMS 50. A ~1 pA Cs^+ primary ion beam was rastered over 10×10 μm^2 areas and secondary ions ($^{12}C^-$, $^{13}C^-$, $^{16}O^-$, $^{17}O^-$, $^{18}O^-$) were collected simultaneously in multicollection mode, along with secondary electrons. Each measurement consisted of 5–10 scans that were added together to form a single image measurement. The data were processed using custom software (Stadermann et al. 2005) and isotopic ratios were calculated by assuming normal bulk isotopic compositions ($^{17}O/^{16}O = 3.6 \times 10^{-4}$; $^{18}O/^{16}O = 1.9 \times 10^{-3}$; McKeegan et al. 2011) for the Acfer 094 matrix material. Grains are considered presolar if their compositions deviate from the average surrounding material by more than 4σ and the anomaly is present in at least three consecutive image layers. Additional details of the measurement and data reduction procedures are described in Floss and Stadermann (2009).

The grains were then analyzed with the Washington University PHI 700 Auger Nanoprobe to determine elemental compositions. Following sputter cleaning with a defocused 2 kV 1 μA Ar^+ beam to remove atmospheric surface contamination, Auger electron energy spectra were obtained with a 10 kV 0.25 nA primary electron beam, following routine procedures developed for the analysis of presolar silicate and oxide grains (Floss and Stadermann 2009; Stadermann et al. 2009). Quantification was carried out using sensitivity factors obtained from a series of olivine and pyroxene standards with variable compositions (Stadermann et al. 2009).

Iron isotopes are typically measured with an O^- primary ion beam, due to their higher ionization yields as positive secondary ions. However, these analyses are technically challenging due to the relatively poor spatial resolution achievable: the diameter of the O^-beam, at ~500 nm, is significantly larger than the majority of the grains, leading to substantial signal contamination from the surrounding isotopically normal grains. Because Fe

is a major element in most presolar silicates, measuring the Fe isotopes as negative secondary ions with the higher spatial resolution of the Cs^+ primary ion beam (~100 nm diameter) can be a viable alternative (e.g., Vollmer and Hoppe 2010), despite the expected lower yields.

We measured the Fe isotopes as oxides in three separate sessions (December 2011, June 2012, and April 2013) using two different experimental setups. In our initial set of analyses, we used two magnetic fields and the following masses: 16 ($^{16}O^-$), 68 ($^{52}Cr^{16}O^-$), 70 ($^{54}Fe^{16}O^-$, $^{54}Cr^{16}O^-$), 73 ($^{57}Fe^{16}O^-$), and 78 ($^{62}Ni^{16}O^-$) were measured in detectors 1–5, followed by 72 ($^{56}Fe^{16}O^-$) and 74 ($^{58}Fe^{16}O^-$, $^{58}Ni^{16}O^-$) in detectors 2–3. Because the signal at mass 74 is completely dominated by the oxide of ^{58}Ni, we did not attempt to measure ^{58}Fe in subsequent measurement sets. All measurements were done in grain mode: following acquisition of a 10×10 μm^2 image of the area of interest, the beam is rastered over individual grains selected from this image. Sizes of the raster boxes varied from 0.05 to 0.34 μm^2, depending on the size of the grain being measured. The measurements were made at a mass resolution high enough ($m/\Delta m \sim 10{,}000$) to achieve partial separation of $^{56}Fe^{16}OH^-$ from $^{57}Fe^{16}O^-$. As shown in Fig. 1, the contribution from $^{56}Fe^{16}OH^-$ to the $^{57}Fe^{16}O^-$ peak is ~1%. However, the hydride contribution appears to be fairly stable, with measurements on an FeNi standard indicating a reproducibility of ~20 ‰ for both $^{57}Fe/^{56}Fe$ and $^{54}Fe/^{56}Fe$. Isotopically normal silicate grains from Acfer 094 matrix material were used as internal standards for the measurements. As discussed in more detail below, the hydride contribution, although greater, again appears to be fairly stable.

The data were normalized to the average compositions of the matrix grains measured in the vicinity of each presolar grain. All data were also examined for signal consistency (e.g., to check for peak shifts that might result in a larger hydride contribution and to remove obvious artifacts in the data due to electronic noise). Corrections were made for ^{54}Cr on ^{54}Fe, based on the measured $^{52}Cr^{16}O^-$ and assuming solar Cr isotopic compositions, and were ≤~10‰ for all of the grains measured. No data are reported for $^{58}Fe/^{56}Fe$, as the $^{58}Fe^{16}O^-$ signal is dominated by contributions from $^{58}Ni^{16}O^-$, as noted above.

RESULTS

We identified a total of 94 O-anomalous presolar grains in our imaging search of Acfer 094 (see Table A1 in the Appendix). Following the classification scheme of Nittler et al. (1997), most of the grains belong to Group 1, with elevated $^{17}O/^{16}O$ ratios and close-to-solar $^{18}O/^{16}O$ (Fig. 2). Another 10 grains belong to Group 4, which are enriched in ^{18}O, with or without concomitant enrichments in ^{17}O. Finally two are Group 3 grains, which are depleted in ^{17}O and ^{18}O. Auger elemental analysis indicates that the majority of the grains are Fe-rich ferromagnesian silicates, with compositions similar to those of other presolar grains from Acfer 094 (Vollmer et al. 2009; Bose et al. 2010). Six grains are Fe-oxides (Table A1).

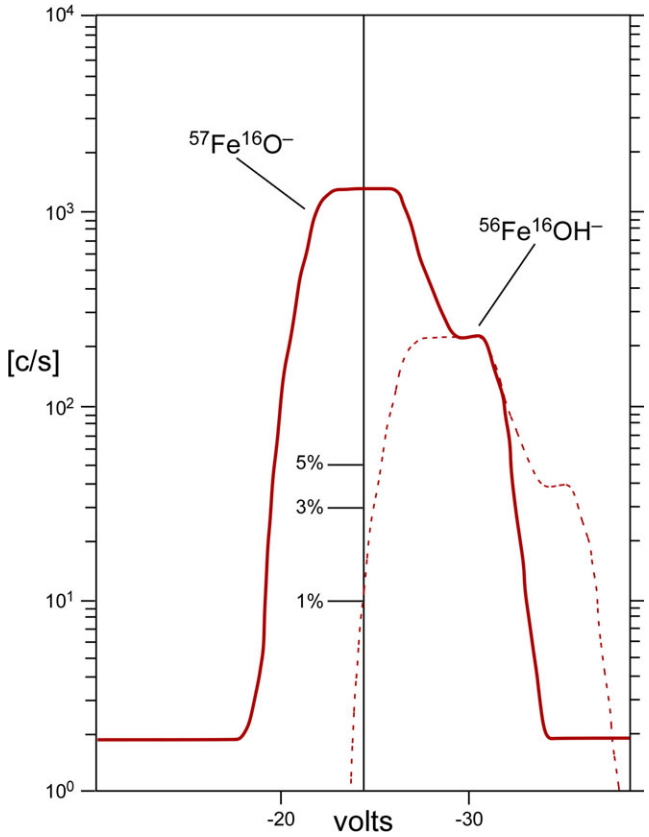

Fig. 1. High mass resolution spectrum at mass 73. The dashed line shows an overlay of the $^{57}Fe^{16}O^-$ peak on the $^{56}Fe^{16}OH^-$ shoulder, indicating a ~1% contribution of the hydride to the signal.

Among the criteria used to select grains for the Fe isotope analyses, we focused in particular on grains that were relatively easy to relocate on the mount and that were at least partially separated from surrounding grains, to minimize signal contamination (e.g., Fig. 3). Table 1 lists the 21 grains measured, along with their sizes and elemental compositions. With the exception of one grain for which we have no compositional information, all of the grains have Fe as a major element, with more Fe than Mg in all but two of the grains; indeed Mg is below detection limits (~3 atom%)

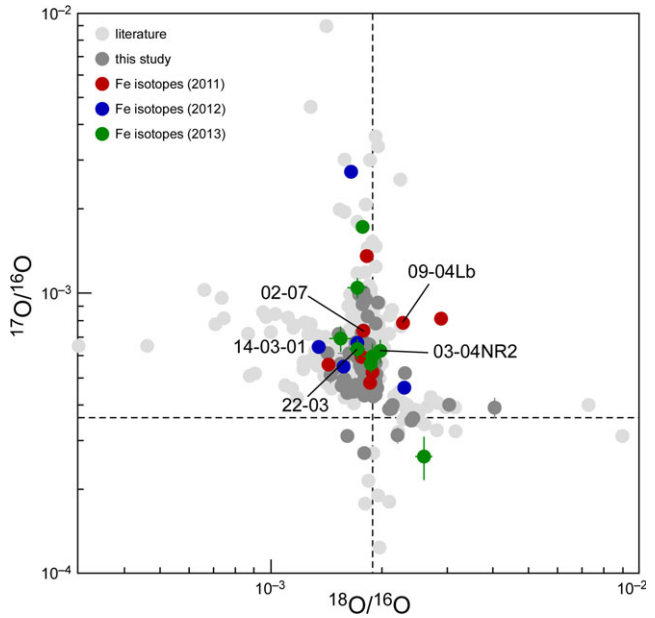

Fig. 2. Oxygen three-isotope plot of presolar grains from Acfer 094. Grains in red, blue, and green were selected for Fe isotope analysis. Grains with anomalous Fe isotopic compositions are labeled. Literature data are from the Presolar Grain Database (Hynes and Gyngard 2009). Errors are 1σ.

in 12 of the grains. Four grains are oxides; the remaining grains are silicates. Aluminum is present in four grains, including one of the oxides. The grains are all half a micron or less in size and most have diameters between 150 and 250 nm; two grains are distinctly elongated (Figs. 3d and 3f). Three of the grains belong to Group 4; the remaining grains belong to Group 1 (Table 2).

The results for the Fe isotopic measurements are presented in Table 2 and Fig. 4. The measured Fe isotopic compositions of normal matrix grains have overall variations on the order of 50–75‰ for both $^{54}Fe/^{56}Fe$ and $^{57}Fe/^{56}Fe$. The $^{54}Fe/^{56}Fe$ ratios of all but one of the presolar grains are consistent with solar values, and the variation in the grains is similar to that seen in the matrix grains. The $^{57}Fe/^{56}Fe$ ratios of the presolar grains show more overall variability but, again, most grains have compositions that are consistent with solar values. Two exceptions are grain WU014-D 02-07, which is depleted in ^{57}Fe ($\delta^{57}Fe/^{56}F = -202 \pm 58‰$; $\delta^{54}Fe/^{56}Fe = -11 \pm 39‰$), and grain WU029-3 03-04NR2, which is depleted in both ^{57}Fe and ^{54}Fe ($\delta^{57}Fe/^{56}Fe = -219 \pm 65‰$; $\delta^{54}Fe/^{56}Fe = -104 \pm 48‰$). Two other grains (WU014-D 09-04Lb and WU029-4 22-03) show modest depletions in ^{57}Fe at the 2–3σ level, and one grain (WU014-B 14-03-01) is slightly enriched in ^{57}Fe (Table 2; Fig. 4).

DISCUSSION

NanoSIMS Analysis of Fe Isotopes: Evaluation

Secondary ion yields in SIMS vary over orders of magnitude for different elements and are influenced by a variety of factors, the most significant of which are ionization potential for positive ions and electron affinity for negative ions. As an electropositive element, Fe is more easily ionized as positive secondary ions than as negative ions and, as noted above, is typically measured with an O^- primary ion beam (e.g., Hinton 1990; Hoppe et al. 2013). Prior to this work, Mostefaoui and Hoppe (2004) and Vollmer and Hoppe (2010) also carried out measurements of the Fe isotopic compositions of presolar silicate grains, using the Cs^+ primary beam of the NanoSIMS and collecting negative secondary ions of the oxides ($^{xx}Fe^{16}O^-$). However, only $^{54}Fe/^{56}Fe$ ratios were reported in these studies. Here, we have demonstrated the feasibility of measuring both $^{54}Fe/^{56}Fe$ and $^{57}Fe/^{56}Fe$ with this approach. While this method provides advantages over similar measurements using the more traditional approach of sputtering with a negative (O^-) primary beam and collecting positive secondary ions, there are also some limitations. We discuss both in more detail below.

As noted earlier, one of the primary advantages of using the Cs^+ primary beam for these measurements is the improved spatial resolution over the O^- beam (~100 nm versus ~500 nm). Because most presolar silicates are on the order of 300 nm or less in diameter and are typically not well separated from surrounding isotopically normal matrix grains, the smaller beam diameter has the potential to significantly reduce the amount of signal contamination introduced during the measurements. We will revisit the question of signal contamination in more detail below. Another notable advantage is the availability of secondary electron images, which greatly simplifies locating the grains for analysis. This is less trivial than it may initially appear. For the most part, the presolar grains are compositionally similar to the surrounding matrix grains and are, therefore, not easily distinguished on the basis of secondary ion images, particularly under the less than optimal imaging conditions available with the O^- beam. Physical characteristics and location relative to fiduciary markers (e.g., Fig. 3) are much more diagnostic, and direct comparison with secondary electron images taken during the initial O isotope mapping is the most straightforward and reliable way to find the grains again for the Fe isotopic analyses.

A trade-off to these advantages is the lower ion yield expected for these measurements. To calculate the

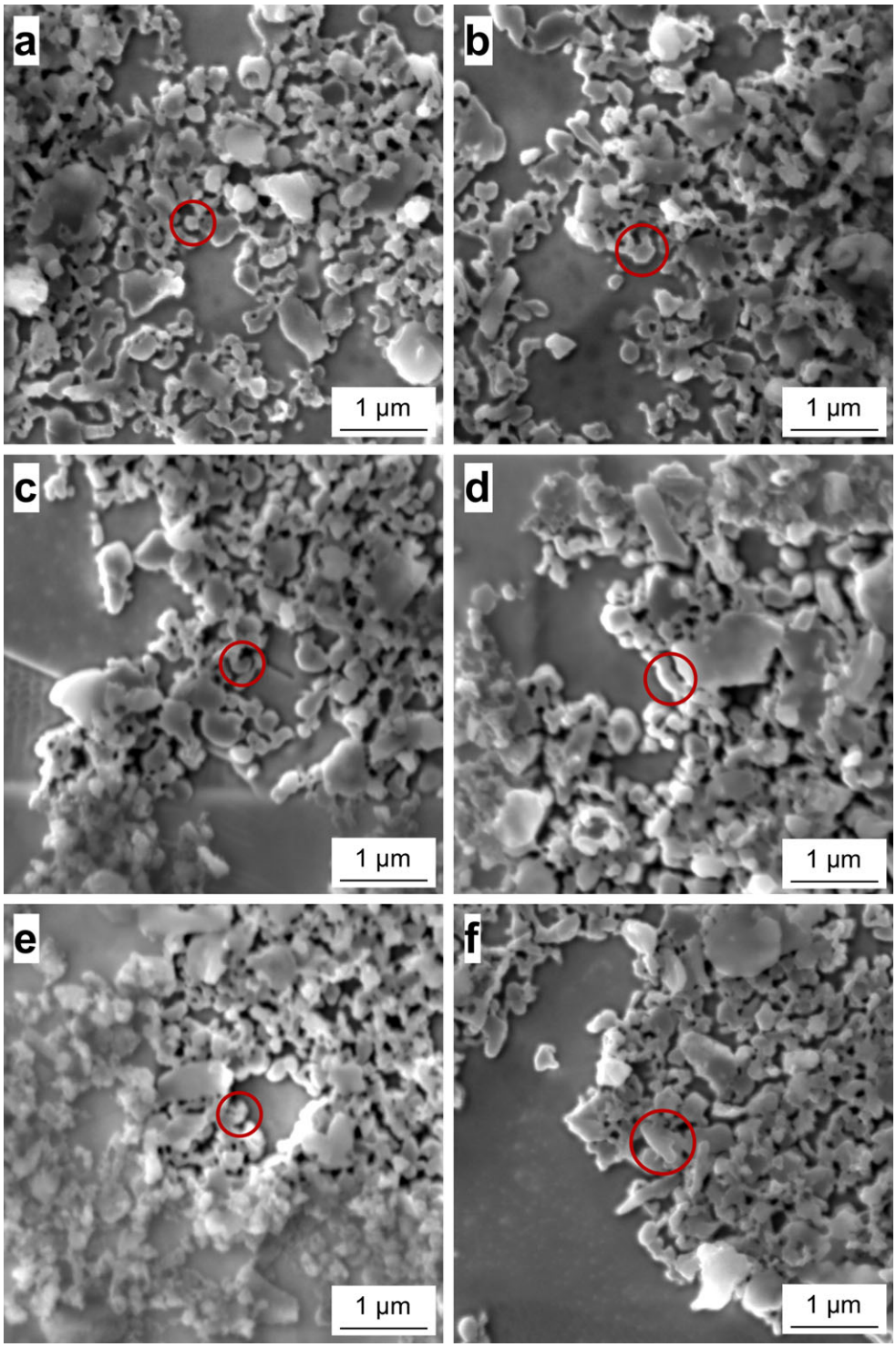

Fig. 3. Secondary electron images of selected O-anomalous presolar grains measured for iron isotopes: a) WU14-D 09-04Lb, b) WU014-D 09-04Ra, c) WU029-3 05-01, d) WU014-B 14-03-01, e) WU029-3 03-04(2), f) WU014-D 02-07.

relative difference in ion yields, we measured the ion intensities of Fe^+ and FeO^- relative to Si in the Acfer 094 matrix grains, which are dominated by silicates broadly similar in composition to the presolar grains of this study. Ion yields in SIMS are determined from the following equation:

Table 1. Sizes and elemental compositions of grains selected for Fe isotopic analysis.

Grain	Size (nm)	O (atom%)	Si (atom%)	Fe (atom%)	Mg (atom%)	Al (atom%)
WU014-D						
02-02	150	n.m.	n.m.	n.m.	n.m.	n.m.
02-06	170	58.4 ± 2.1	12.1 ± 1.3	17.8 ± 2.0	b.d.	11.8 ± 2.9
02-07	270 × 680	56.1 ± 2.0	15.0 ± 1.7	15.1 ± 1.7	13.9 ± 1.3	b.d.
09-04Lb	170	54.3 ± 2.0	23.3 ± 2.6	22.4 ± 2.5	b.d.	b.d.
09-04Ra	290	55.8 ± 2.0	20.0 ± 2.2	10.0 ± 1.1	14.2 ± 1.3	b.d.
10-06T	150	53.8 ± 1.9	19.7 ± 2.2	15.9 ± 1.8	b.d.	10.6 ± 2.6
16-08	150	58.2 ± 2.1	10.6 ± 1.2	31.2 ± 3.5	b.d.	b.d.
16-12	170	57.3 ± 2.1	b.d.	42.7 ± 4.8	b.d.	b.d.
WU014-B						
05-01-01	270	55.5 ± 2.0	16.9 ± 1.9	15.1 ± 1.7	12.5 ± 1.2	b.d.
09-10-01	200	60.6 ± 2.2	12.0 ± 1.3	14.4 ± 1.6	13.0 ± 1.2	b.d.
12-05-01	360	60.7 ± 2.2	b.d.	39.3 ± 4.4	b.d.	b.d.
14-03-01	220 × 340	64.3 ± 2.3	13.3 ± 1.5	22.4 ± 2.5	b.d.	b.d.
16-04-01	250	54.3 ± 2.0	16.6 ± 1.8	19.2 ± 2.2	10.0 ± 0.9	b.d.
WU029-3						
03-04(1)	150	50.4 ± 1.8	24.5 ± 2.7	25.1 ± 2.8	b.d.	b.d.
03-04(2)	180	58.6 ± 2.1	b.d.	21.6 ± 2.4	b.d.	19.8 ± 4.9
05-01	170	60.1 ± 2.2	16.8 ± 1.8	8.9 ± 1.0	14.1 ± 1.3	b.d.
05-04	250	48.1 ± 1.7	17.6 ± 1.9	34.3 ± 3.8	b.d.	b.d.
06-03	220	45.0 ± 1.6	20.6 ± 2.3	16.7 ± 1.9	17.8 ± 1.7	b.d.
09-04	240	53.5 ± 1.9	27.5 ± 3.0	19.0 ± 2.1	b.d.	b.d.
WU029-4						
12-03	220	40.3 ± 1.5	29.6 ± 3.3	10.7 ± 1.2	9.5 ± 0.9	9.9 ± 2.5
22-03	200	58.6 ± 2.1	b.d.	41.4 ± 4.6	b.d.	b.d.

$$Y_i = W_i/W_{Si} * 1/F_i \quad (1)$$

where Y is the ion yield of element i, W is the atomic weight of element i or Si, and F_i is the sensitivity factor of element i relative to Si. The sensitivity factor, F_i, relates ion intensities to concentrations as follows:

$$I_i/I_{Si} = 1/F_i * C_i/C_{Si} \quad (2)$$

where I is the ion intensity of element i or Si, and C is the concentration of element i or Si. Combining Equations and gives:

$$Y_{FeO^-}/Y_{Fe^+} = W_{FeO^-}/W_{Fe^+} * I_{FeO^-}/I_{Si^-} * I_{Si^+}/I_{Fe^+} \quad (3)$$

The ion intensities, I_{Fe^+}/I_{Si^+} and I_{FeO^-}/I_{Si^-}, determined from our measurements are 4.0 ± 0.2 and 0.23 ± 0.02, respectively, resulting in a relative ion yield of FeO^- to Fe^+ of 0.07, or a factor of 14 reduction. However, as noted earlier, this large loss in signal intensity is compensated for by the high concentrations of Fe in the majority of these grains. Indeed, errors on the $^{54}Fe/^{56}Fe$ and $^{57}Fe/^{56}Fe$ ratios due to counting statistics were less than 5% in the vast majority of the measurements. Thus, while clearly not suitable for grains in which Fe is a trace element (e.g., presolar SiC), for presolar silicate grains with Fe as a major element, the lower ion yield obtained by measuring positive secondary ions is not a serious limitation.

Another area of potential concern is the incomplete separation of $^{57}Fe^{16}O^-$ from $^{56}Fe^{16}OH^-$ at mass 73. As shown in Fig. 1, the contribution from the ^{56}FeO hydride is about 1% for measurements done on an FeNi standard. The hydride contribution is greater for the analyses of the Acfer 094 grains, with similar count rates for both peaks, reflecting the increased amount of oxygen present in the silicate grains compared to the FeNi standard. However, if the hydride contribution is similar in the different grains, as it is for measurements on the FeNi standard, the additional contribution will not affect the measured $^{57}Fe/^{56}Fe$ ratios, as compositions are normalized to the matrix grains in the vicinity of each presolar grain measured. As shown in Fig. 4, although the reproducibility among the isotopically normal matrix grains is more variable overall than that observed on the FeNi standard, it is again similar for both $^{57}Fe/^{56}Fe$ and $^{54}Fe/^{56}Fe$ (~50–75‰), indicating a relatively stable hydride contribution in the different grains. Moreover, Fig. 5 shows that there is no correlation between the Fe isotopic compositions measured in the matrix grains and their

Table 2. Isotopic compositions of grains selected for Fe isotopic analysis.

Grain	Group	$^{17}O/^{16}O$ ($\times10^{-4}$)	$^{18}O/^{16}O$ ($\times10^{-3}$)	$\delta^{54}Fe/^{56}Fe$ (‰)	$\delta^{57}Fe/^{56}Fe$ (‰)	$^{16}O^-/^{56}Fe^{16}O^-$
WU014-D (2011)						
02-02	4	8.08 ± 0.45	2.89 ± 0.08	42 ± 30	−21 ± 42	14.9
02-06	1	5.90 ± 0.34	1.76 ± 0.06	−33 ± 33	−85 ± 48	13.5
02-07	1	7.31 ± 0.21	1.78 ± 0.03	−11 ± 29	−202 ± 58	19.6
09-04Lb	1	7.80 ± 0.37	2.28 ± 0.06	22 ± 37	−106 ± 40	14.9
09-04Ra	1	5.53 ± 0.29	1.43 ± 0.05	−3 ± 32	27 ± 49	10.6
10-06T	1	13.5 ± 0.5	1.82 ± 0.05	−7 ± 59	5 ± 66	17.9
16-08	1	4.77 ± 0.26	1.85 ± 0.05	57 ± 35	50 ± 39	19.1
16-12	1	5.20 ± 0.22	1.88 ± 0.04	3 ± 64	−36 ± 75	9.8
WU014-B (2012)						
05-01-01	1	27.0 ± 0.4	1.65 ± 0.04	−30 ± 56	41 ± 53	13.8
09-10-01	1	5.44 ± 0.16	1.57 ± 0.03	−17 ± 33	−72 ± 51	13.4
12-05-01	4	4.58 ± 0.12	2.30 ± 0.03	10 ± 19	33 ± 35	10.9
14-03-01	1	6.40 ± 0.27	1.35 ± 0.04	−39 ± 51	109 ± 60	13.2
16-04-01	1	6.61 ± 0.36	1.72 ± 0.06	42 ± 48	7 ± 57	12.1
WU029-3 (2013)						
03-04(1)	4	2.60 ± 0.46	2.60 ± 0.14	−26 ± 47	48 ± 75	9.3
03-04(2)	1	6.19 ± 0.60	1.98 ± 0.10	−104 ± 48	−219 ± 65	7.5
05-01	1	10.4 ± 0.9	1.71 ± 0.11	43 ± 54	44 ± 86	8.3
05-04	1	17.2 ± 0.6	1.77 ± 0.06	−40 ± 27	−30 ± 33	9.7
06-03	1	5.58 ± 0.41	1.87 ± 0.06	13 ± 50	−82 ± 79	10.9
09-04	1	5.92 ± 0.66	1.88 ± 0.11	4 ± 40	15 ± 93	11.7
WU029-4 (2013)						
12-03	1	6.86 ± 0.72	1.54 ± 0.11	3 ± 32	37 ± 60	9.2
22-03	1	6.29 ± 0.53	1.72 ± 0.08	13 ± 38	−130 ± 76	8.7

$^{16}O^-/^{56}Fe^-$ ion ratios. If the variations in the $^{57}Fe/^{56}Fe$ ratios observed in the normal matrix grains were due to variable contributions of the ^{56}FeO hydride, we would expect more variability in the $^{57}Fe/^{56}Fe$ ratios than in the $^{54}Fe/^{56}Fe$ ratios, along with a positive correlation between the $^{16}O^-/^{56}Fe^-$ ion ratios and the $^{57}Fe/^{56}Fe$ compositions, which are not observed. The two presolar grains with significant (and similar) depletions in ^{57}Fe have $^{16}O^-/^{56}Fe^-$ ion ratios that do not differ substantially from those of the matrix grains to which these grains are normalized, confirming that the depletions are not due to the normalization procedure.

Finally, we return to the question of signal contamination from surrounding isotopically normal grains. Nguyen et al. (2007) presented a detailed analysis of the degree to which the oxygen isotopic compositions of presolar silicate and oxide grains are affected by isotopic dilution during raster ion imaging of densely packed grains. The simulations, carried out for measurements done with the NanoSIMS Cs^+ primary beam, demonstrated that isotopic dilution affected all grains, including those significantly larger than the primary beam, and was particularly severe for the smallest grains (with diameters of ~150 nm). Nguyen et al. (2007) concluded that all O isotopic anomalies determined using raster ion imaging must be considered lower limits, and estimated that as many as half of all Group 1 grains with diameters of 250 nm may not be identified as presolar during such measurements. From this analysis, it is clear that although the use of the Cs^+ primary beam will reduce the amount of signal contamination, compared to measurements done with the O^- beam, it will not eliminate it completely.

The degree to which isotopic dilution may have affected the Fe isotopic compositions of our grains is difficult to determine quantitatively. The Fe isotopes in this study were not measured using raster ion imaging but, instead, were done in grain mode, in which the grains are individually selected for analysis from a larger raster ion image of the area of interest. In addition to factors such as beam size and shape (e.g., Nguyen et al. 2007), the amount of signal contamination from surrounding grains depends on things such as the size of the raster box selected relative to the size of the grain, how well the box is centered on the grain, and the extent to which the grain is surrounded by other Fe-rich isotopically normal grains (as noted above, we attempted to select grains that were at least partially separated from the surrounding grains, although this was not always possible). As we know the sizes of the grains and the sizes of the raster boxes used

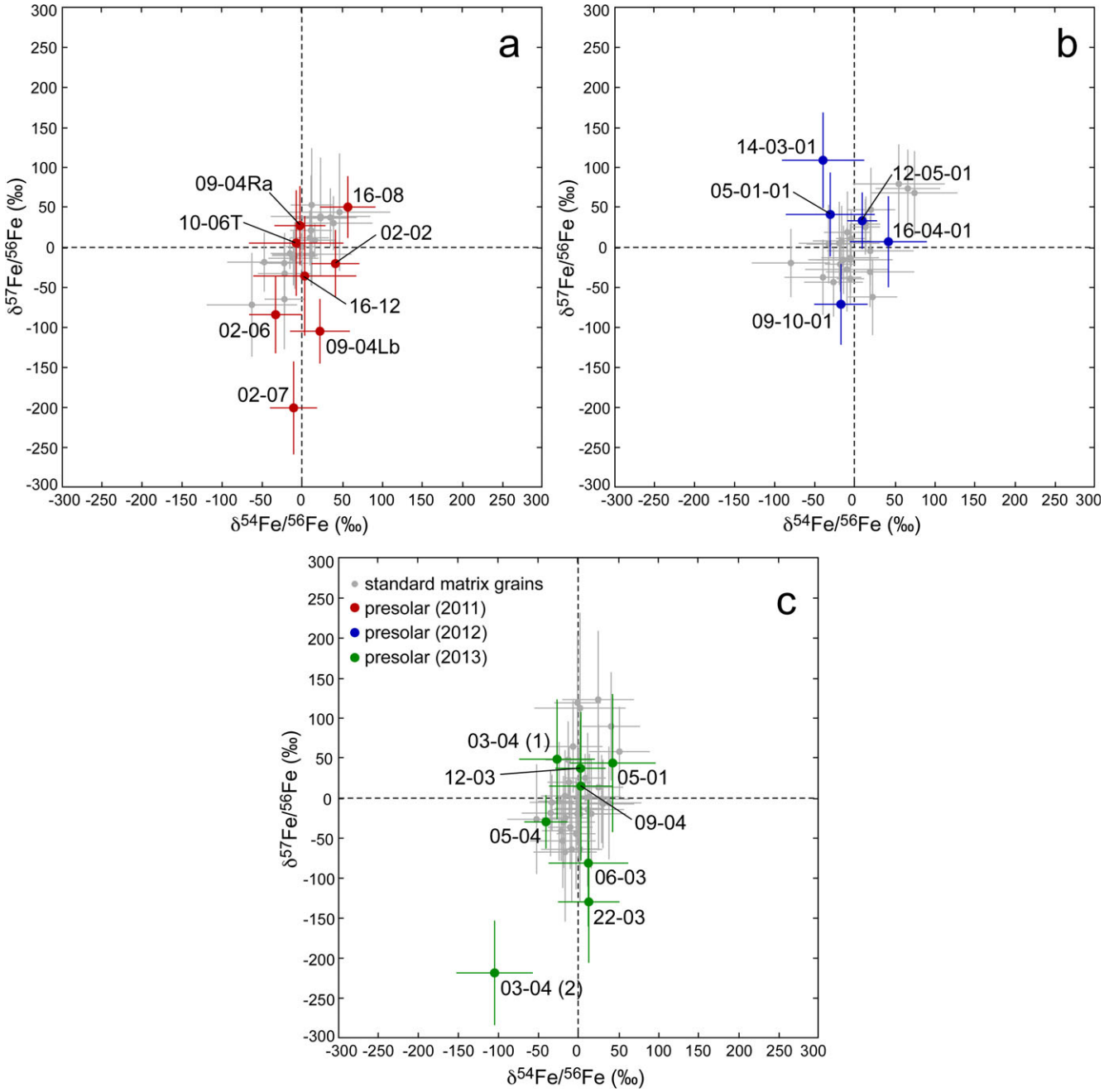

Fig. 4. Iron three-isotope ($^{54}Fe/^{56}Fe$ and $^{57}Fe/^{56}Fe$, plotted as permil deviations from normal) plots of O-anomalous grains from Acfer 094: a) data from December 2011, b) data from June 2012, c) data from April 2013. Standard matrix grains, also from Acfer 094, are shown in gray. Errors are 1σ.

for the measurements, we can calculate what fraction of each measurement area consisted of the grain of interest. The results show that the presolar grains typically comprise between 30% and 50% of the measurement areas, although in a few cases, the fractions were as low as 15% or as high as 100%. Thus, it is clear that a substantial fraction of the Fe signal contributing to the measured compositions comes from the surrounding grains, even with the improved spatial resolution of the Cs^+ beam.

Many of the grains selected in this study were relatively small, ~200 nm or less (Table 1), and it was often difficult to precisely select and center the raster box on the grains. To some extent, it may be possible to mitigate this in future measurements through the use of newer software that allows grains to be selected more

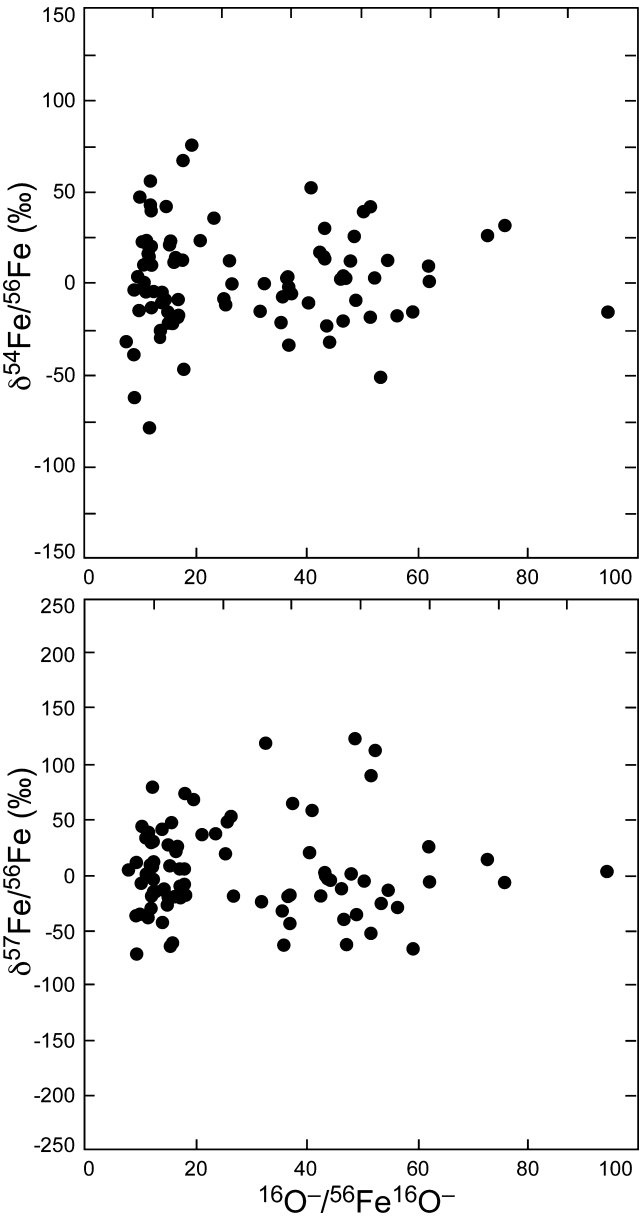

Fig. 5. Oxygen to iron ion ratios versus $\delta^{54}Fe/^{56}Fe$ (top) and $\delta^{57}Fe/^{56}Fe$ (bottom) in isotopically normal matrix grains from Acfer 094.

precisely (e.g., through manual outlining of regions of interest). Nevertheless, it will remain important, as much as possible, to select larger grains for such analyses. The largest grain measured in this study, WU014-D 02-07 (270×680 nm^2), is one of the two grains with clear ^{57}Fe depletions (Table 2; Fig. 2) and is the only grain for which the defined raster area is smaller than the size of the grain. The other clearly ^{57}Fe-depleted grain, WU029-3 03-04NR2, is significantly smaller and, based on the size of the measurement area, its true isotopic composition is likely to be a factor of 2–3 more anomalous than the measured composition shown in Table 2 and Fig. 2. Similarly, grains WU014-D 09-04Lb and WU029-4 22-03, which are modestly depleted in ^{57}Fe, and WU014-B 14-03-01, which is enriched in ^{57}Fe, all have grain areas that are smaller than the measurement areas and likely have true isotopic compositions that are factors of 2–3 more anomalous than the measured compositions.

Origin of Fe in Presolar Silicates

Several studies have discussed possible scenarios to account for the high Fe abundances observed in many presolar silicates (Nguyen et al. 2007, 2010; Floss and Stadermann 2009; Vollmer et al. 2009; Bose et al. 2010). Secondary alteration has clearly played a role in some meteorites such as Adelaide, which shows evidence of Fe enrichment due to thermal annealing (Floss and Stadermann 2012), and MIL 07687, in which some Fe appears to have been leached from presolar silicates during aqueous alteration (Floss and Brearley 2015). However, most of the meteorites with high presolar silicate abundances, including Acfer 094, show little evidence of alteration, suggesting that much of the Fe present in the grains is primary. Indeed the anomalous Fe isotopic compositions in several of the presolar silicate grains studied here are clear evidence of a primary origin for the Fe in these grains. Elevated Fe abundances are probably due to nonequilibrium condensation of the grains in the stellar envelopes where they formed (e.g., Gail and Sedlmayr 1999; Ferrarotti and Gail 2001). Most silicate dust forms during short high mass-loss episodes that occur after thermal pulses in thermally pulsing AGB stars (Gail et al. 2009). The stellar environment during these episodes will be highly variable, with strong stellar winds and temperature drops, leading to grain formation under kinetic conditions. The modeling work of Gail et al. (2009) suggests that silicate dust should consist of a mixture of olivine and pyroxene, with an average mole fraction of the Mg-rich component of about 0.6, consistent with the Fe-rich compositions of many presolar silicates. Thus, although there are exceptions, on balance it seems likely that secondary processing had a limited role in establishing the high Fe contents of most presolar silicate grains.

Isotopic Compositions—AGB Stars

Most (18 of 21) of the grains for which we measured the Fe isotopes have Group 1 oxygen isotopic compositions, indicating origins in low-mass RGB and AGB stars of close-to-solar metallicity (e.g., Boothroyd et al. 1994; Nittler et al. 2008). Hydrogen burning

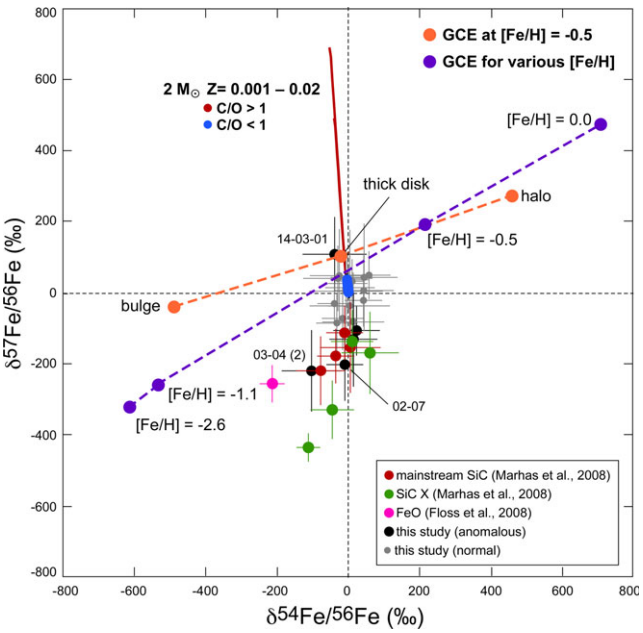

Fig. 6. Iron three-isotope ($^{54}Fe/^{56}Fe$ and $^{57}Fe/^{56}Fe$, plotted as permil deviations from normal) plot of O-anomalous grains from Acfer 094 (this study; Floss et al. 2008) and SiC grains from Murchison (Marhas et al. 2008). Errors are 1σ. Also shown are model predictions for 2 $M_\odot$ AGB stars with metallicities from 0.001 to 0.02 (Cristallo et al. 2011), and for the evolution of the Fe isotopes in the Galaxy (Kobayashi et al. 2011). See text for details.

during the CNO cycle produces ^{17}O and destroys ^{18}O. As a star moves off of the main sequence to the red giant and asymptotic giant branch phases, convection dredges this material up to the surface where grain formation takes place, resulting in enhanced $^{17}O/^{16}O$ ratios and $^{18}O/^{16}O$ ratios that are slightly depleted relative to the initial compositions of the star. The five grains from our study that show evidence for anomalous Fe isotopic compositions all belong to group 1 (e.g., Fig. 2). They are shown in Fig. 6, along with model predictions for Fe nucleosynthesis. The largest compositional changes take place during the AGB phase, when thermal pulses drive nucleosynthesis and convective mixing episodes bring newly synthesized material to the star's surface (e.g., Busso et al. 1999; Herwig 2005; Karakas and Lattanzio 2014). Cristallo et al. (2011) systematically investigated the evolution of low-mass AGB stars and calculated stellar yields for a series of masses and metallicities; the results of their calculations are accessible at the FRUITY (FRANEC Repository of Updated Isotopic Tables and Yields) database. For the Fe isotopes, neutron capture in the He intershell, from either the $^{13}C(\alpha, n)^{16}O$ or $^{22}Ne(\alpha,n)^{25}Mg$ neutron sources, leads to the destruction of ^{54}Fe and the production of ^{57}Fe and ^{58}Fe. Thus, $^{54}Fe/^{56}Fe$ ratios are not expected to change substantially from the initial values of the parent stars, whereas the $^{57}Fe/^{56}Fe$ and $^{58}Fe/^{56}Fe$ ratios will be elevated. Figure 6 shows the isotopic compositions expected in the envelope during the third dredge-up for 2 $M_\odot$ AGB stars with metallicities from 0.001 to 0.02. The models predict slight depletions in ^{54}Fe and maximum enrichments of up to ~700‰ for ^{57}Fe. However, in the early dredge-up episodes where the C/O ratios are <1 and O-rich grains are more likely to form, the maximum enrichments in ^{57}Fe are less, on the order of about 50‰.

The normal $^{54}Fe/^{56}Fe$ ratios in most of our Group 1 grains are consistent with the data obtained by Vollmer and Hoppe (2010) for most of their Group 1 grains, and indicate that these grains originated from parent stars with close-to-solar metallicities. Vollmer and Hoppe (2010) also report one Group 1 grain that is enriched in ^{54}Fe, but note that no correction for ^{54}Cr was made for that grain, suggesting that the excess ^{54}Fe was likely an analytical artifact. Many of our Group 1 grains also have normal $^{57}F/^{56}Fe$ ratios, in agreement with the model predictions; the slight ^{57}Fe enrichment observed in grain 14-03-1 is also consistent with the isotopic composition expected following early dredge-up episodes. However, the depletions in ^{57}Fe that we observe in several grains, most notably grains 02-07 and 03-04 (2), are not predicted by current AGB models. Marhas et al. (2008) measured the Fe isotopic compositions of SiC grains of AGB origin (e.g., mainstream SiC). While many of the grains exhibited solar $^{54}Fe/^{56}Fe$ and $^{57}Fe/^{56}Fe$ ratios, four grains showed deficits in ^{57}Fe similar to those observed in our silicates (Fig. 6). As SiC grains form later during the AGB phase than O-rich grains (i.e., when C/O > 1), the discrepancy with model predictions is even greater (Fig. 6). In addition to being depleted in ^{57}Fe, grain 03-04 (2) shows a moderate (2σ) depletion in ^{54}Fe. Marhas et al. (2008) also observed ^{54}Fe depletions in two SiC grains from AGB stars, and Vollmer and Hoppe (2010) identified one extremely ^{17}O-rich grain that was depleted in ^{54}Fe. These authors suggested that heterogeneous galactic evolution could account for minor deficits in ^{54}Fe. However, the ^{57}Fe deficits of these grains are not easily accounted for in this way (see below) and, thus, remain unexplained.

Isotopic Compositions—Type II Supernovae

The remaining three grains for which we measured the Fe isotopes, 02-02, 12-05-1, and 03-04(1), belong to Group 4. All three have normal $^{54}Fe/^{56}Fe$ and $^{57}Fe/^{56}Fe$ ratios, as do three Group 4 grains analyzed by Nguyen and Messenger (2014). Figure 7 shows the distribution of O and Fe isotopes in the interior zones of a 15 $M_\odot$

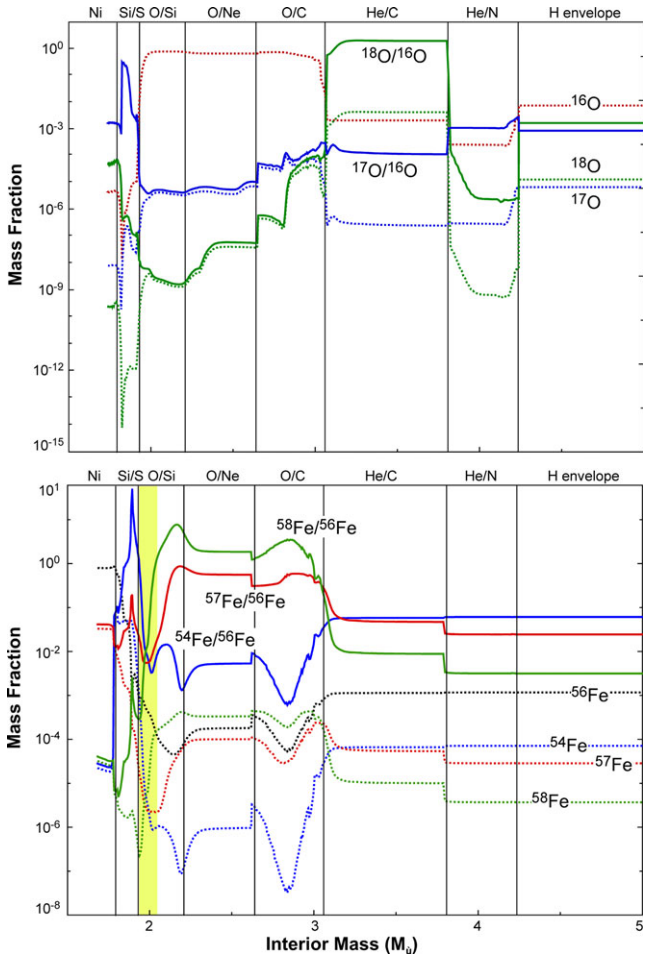

Fig. 7. Oxygen and iron isotopic compositions in the interior zones of a 15 $M_\odot$ supernova model (Rauscher et al. 2002). The yellow-shaded area shows the portion of the O/Si zone in which both ^{54}Fe and ^{57}Fe are depleted. See text for details.

supernova model (Rauscher et al. 2002). The O isotopic compositions of these grains suggest formation in the H envelope with some contribution from the He/C zone, which is enriched in ^{18}O. The Fe isotope ratios are normal in the He/N zone and H envelope and close-to-normal in the He/C zone, consistent with the Fe isotopic compositions of these grains. However, based on analyses of multiple isotopic systems, Nguyen and Messenger (2014) found that contributions from the Si/S zone were required to reproduce the grain compositions, leading to excesses in ^{54}Fe that were not observed in their grains. A similar problem exists with SiC X grains, which require a contribution from the Si/S zone to account for observed ^{28}Si enrichments, but also do not show the concomitant excesses in ^{54}Fe (Marhas et al. 2008). An excess in ^{54}Fe, consistent with a contribution from the inner zones of a supernova, was observed in a Group 4 silicate measured by Mostefaoui and Hoppe (2004).

Like some of the AGB grains discussed above, supernova grains with deficits in ^{57}Fe have been reported (Floss et al. 2008; Marhas et al. 2008). A Group 4 FeO grain, 34C-10, shows significant depletions in both ^{54}Fe and ^{57}Fe (Floss et al. 2008), and four SiC X grains have deficits in ^{57}Fe (Marhas et al. 2008); one of these is also depleted in ^{54}Fe (Fig. 6). ^{54}Fe is depleted in the O/Si, O/Ne, and O/C zones, but ^{57}Fe is enriched in most of these zones. The only region with depletions in both of these isotopes is a small pocket in the O/Si zone (Fig. 7). Mixing with this pocket can reproduce the Fe isotopic composition of grain 34C-10, but leads to depleted $^{18}O/^{16}O$ and $^{17}O/^{16}O$ compositions, because this zone is strongly enriched in ^{16}O. Both the O and Fe isotopic compositions could be explained if the grain condensed initially in the O/Si zone as Fe metal and was later oxidized to FeO in an ^{18}O-rich environment. However, it is unlikely that reduced Fe metal would condense in such an O-rich zone. Similar problems exist with the ^{57}Fe-depleted SiC X grains, which are also not likely to condense in the O-rich O/Si zone where ^{57}Fe depletions are observed (Marhas et al. 2008). Thus, as for the grains of AGB star origin, current models are unable to account for the compositions of these grains.

Galactic Chemical Evolution

Galactic chemical evolution (GCE) has been invoked to account for the spread of Si isotopic compositions observed in mainstream SiC grains of AGB origin (Timmes and Clayton 1996; Alexander and Nittler 1999) and presolar silicate grains of RGB/AGB origin (Nguyen et al. 2007, 2010; Vollmer et al. 2008). Rather than resulting from nucleosynthetic processes in the stars, the isotopic ratios of the grains reflect the initial compositions of their parent stars, and the observed compositional ranges indicate the contribution of grains from stars with different metallicities to the solar system inventory. As discussed above, the *s*-process contribution to Fe is smaller for silicates than it is for SiC and, thus, Fe isotopic measurements in presolar silicates should provide tighter constraints for galactic chemical evolution studies. Kobayashi et al. (2011) modeled the evolution of isotope ratios in the Milky Way galaxy. Figure 6 shows the galactic evolution of Fe isotopes for different regions of the galaxy and for a range of metallicities in the solar neighborhood. Because formation of the primary isotope (here ^{56}Fe) is independent of metallicity while production of the secondary isotopes (^{54}Fe and ^{57}Fe) depends on the presence of the primary isotope, galactic evolution will lead to higher ratios of $^{54}Fe/^{56}Fe$ and $^{57}Fe/^{56}Fe$ (Fig. 6). Most of the grains from our study

and from those of others (Marhas et al. 2008; Vollmer and Hoppe 2010; Nguyen and Messenger 2014) have Fe isotopic compositions consistent, within errors, with parent stars of metallicity [Fe/H] ~ −0.5 in the galactic disk. However, grains with ^{57}Fe depletions fall below the galactic evolution line. The discrepancy is not resolved by invoking origins in lower metallicity stars because the grains do not exhibit the accompanying large depletions in ^{54}Fe.

One of the central implications of galactic chemical evolution is a homogeneous evolution of the age–metallicity relationship (e.g., Timmes and Clayton 1996). However, observational data of this relationship in the galaxy show significant scatter (Nittler 2005), suggesting that processes for heterogeneous mixing must play a role in GCE as well (e.g., Malinie et al. 1993; Copi 1997; Van den Hoek and de Jong 1997). Nittler (2005) explored heterogeneous galactic evolution through constraints provided by presolar oxide and SiC stardust. The results of that study suggested a well-mixed interstellar medium and that the scatter in the age–metallicity relationship observed for disk stars could not be explained by heterogeneous mixing of stellar ejecta (Nittler 2005). Similarly, heterogeneous galactic evolution could not account for the wide range of ^{18}O/^{16}O ratios observed in presolar oxide grains (and by analogy presolar silicates), implying that these grains either formed in stars with a factor of three greater range in metallicity than SiC grains from similar types of stars, or that limited cool bottom processing led to the wider range of ^{18}O/^{16}O ratios (Nittler 2005). Trappitsch et al. (2013) extended this model to the Fe isotopes, but with inconclusive results, due to the limited amount of grain data available to date.

CONCLUSIONS

We have demonstrated that the Fe isotopic compositions (^{54}Fe/^{56}Fe and ^{57}Fe/^{56}Fe) of presolar silicate grains with high Fe contents can be determined by measuring the Fe isotopes as negative secondary oxides with the Cs^+ primary ion beam on the NanoSIMS. These measurements allow a reduced level of contamination from surrounding isotopically normal silicates, compared to the larger O^- primary beam, and allow easier relocation of the grains in the matrix areas of thin sections and dense grain size separates in which these grains are normally identified.

We analyzed 21 presolar silicate and oxide grains using this approach. The majority of the grains have solar Fe isotopic compositions within errors, consistent with their origins in AGB stars or the ejecta of Type II supernovae. However, four Group 1 grains show depletions in ^{57}Fe that are inconsistent with predictions from current models of stellar nucleosynthesis and galactic evolution. Additional modeling is needed to understand the origins of such grains, as wells as some presolar SiC grains that are similarly depleted in ^{57}Fe.

Acknowledgments—We are grateful to two anonymous reviewers for constructive comments that significantly improved this work. We also thank F. Gyngard for assistance with the NanoSIMS measurements. This work was funded by NASA grants NNX10AH43G and NNX14AG25G to C. F.

Editorial Handling—Dr. A. J. Timothy Jull

REFERENCES

Alexander C. M. O'D. and Nittler L. R. 1999. The galactic evolution of Si, Ti and O isotopic ratios. *The Astrophysical Journal* 519:222–235.

Amari S., Lewis R. S., and Anders E. 1994. Interstellar grains in meteorites. I-Isolation of SiC, graphite, and diamond; size distributions of SiC and graphite. *Geochimica et Cosmochimica Acta* 58:459–470.

Boothroyd A. I., Sackmann I. J., and Wasserburg G. J. 1994. Predictions of oxygen isotope ratios in stars and of oxygen-rich interstellar grains in meteorites. *The Astrophysical Journal* 430:L77–L80.

Bose M., Floss C., and Stadermann F. J. 2010. An investigation into the origin of Fe-rich presolar silicates in Acfer 094. *The Astrophysical Journal* 714:1624–1636.

Bose M., Floss C., Stadermann F. J., Stroud R. M., and Speck A. K. 2012. Circumstellar and interstellar material in the CO3 chondrite ALHA77307: An isotopic and elemental investigation. *Geochimica et Cosmochimica Acta* 93:77–101.

Busso M., Gallino R., and Wasserburg G. J. 1999. Nucleosynthesis in asymptotic giant branch stars: Relevance for galactic enrichment and solar system formation. *Annual Review in Astronomy and Astrophysics* 37:239–309.

Copi C. J. 1997. A stochastic approach to chemical evolution. *The Astrophysical Journal* 487:704–718.

Cristallo S., Piersanti L., Straniero O., Gallino R., Dominguez I., Abia C., Di Rico G., Quintini M., and Bisterzo S. 2011. Evolution, nucleosynthesis, and yields of low-mass asymptotic giant branch stars at different metallicities. II. The FRUITY database. *The Astrophysical Journal Supplement* 197:1–21, doi:10.1088/0067-0049/197/2/17.

Ferrarotti A. S. and Gail H.-P. 2001. Mineral formation in stellar winds II. Effects of Mg/Si abundance variations on dust composition in AGB stars. *Astronomy & Astrophysics* 371:133–151.

Floss C. and Brearley A. J. 2015. Effects of secondary processing on presolar grain abundances and compositions in the unique carbonaceous chondrite Miller Range 07687 (abstract #1004). 46th Lunar and Planetary Science Conference. CD-ROM.

Floss C. and Stadermann F. J. 2009. Auger nanoprobe analysis of presolar ferromagnesian silicate grains from

primitive CR chondrites QUE 99177 and MET 00426. *Geochimica et Cosmochimica Acta* 73:2415–2440.

Floss C. and Stadermann F. J. 2012. Presolar silicate and oxide abundances and compositions in the ungrouped carbonaceous chondrite Adelaide and the K chondrite Kakangari: The effects of secondary processing. *Meteoritics & Planetary Science* 47:992–1009.

Floss C., Stadermann F. J., and Bose M. 2008. Circumstellar Fe oxide from the Acfer 094 carbonaceous chondrite. *The Astrophysical Journal* 672:1266–1271.

Floss C., Ong W. J., and Gyngard F. 2012. Iron isotopic compositions of presolar silicate grains from Acfer 094 (abstract #5031). *Meteoritics & Planetary Science* 47:A96.

Gail H.-P. and Sedlmayr E. 1999. Mineral formation in stellar winds I. Condensation sequence of silicate and iron grains in stationary oxygen rich outflows. *Astronomy & Astrophysics* 347:594–616.

Gail H.-P., Zhukovska S. V., Hoppe P., and Trieloff M. 2009. Stardust from asymptotic giant branch stars. *The Astrophysical Journal* 698:1136–1154.

Herwig F. 2005. Evolution of asymptotic giant branch stars. *Annual Reviews in Astronomy & Astrophysics* 43:435–479.

Hinton R. W. 1990. Ion microprobe trace-element analysis of silicates: Measurement of multi-element glasses. *Chemical Geology* 83:11–25.

Hoppe P., Cohen S., and Meibom A. 2013. NanoSIMS: Technical aspects and applications in cosmochemistry and biological geochemistry. *Geostandards & Geoanalytical Research* 37:111–154.

Hynes K. M. and Gyngard F. 2009. The presolar grain database: http://presolar.wustl.edu/~pgd (abstract #1198). 40th Lunar and Planetary Science Conference. CD-ROM.

Karakas A. I. and Lattanzio J. C. 2014. The Dawes review II: Nucleosynthesis and stellar yields of low and intermediate-mass single stars. *Publications of the Astronomical Society of Australia* 31:1–62, doi:10.1017/pasa.2014.21.

Kobayashi C., Karakas A. I., and Umeda H. 2011. The evolution of isotope ratios in the Milky Way galaxy. *Monthly Notices of the Royal Astronomical Society* 414:3231–3250.

Malinie G., Hartmann D. H., Clayton D. D., and Matthews G. J. 1993. Inhomogeneous chemical evolution of the galactic disk. *The Astrophysical Journal* 413:633–640.

Marhas K. K., Amari S., Gyngard F., Zinner E., and Gallino R. 2008. Iron and nickel isotopic ratios in presolar SiC grains. *The Astrophysical Journal* 689:622–645.

McKeegan K. D., Kallio A. P. A., Heber V. S., Jarzebinski G., Mao P. H., Coath C. D., Kunihiro T., Wiens R. C., Nordholt J. E., Moses R. W. Jr., Reisenfeld D. B., Jurewicz A. J. G., and Burnett D. S. 2011. The oxygen isotopic composition of the Sun inferred from captured solar wind. *Science* 332:1528–1532.

Messenger S., Keller L. P., Stadermann F. J., Walker R. M., and Zinner E. 2003. Samples of stars beyond the solar system: Silicate grains in interplanetary dust. *Science* 300:105–108.

Messenger S., Keller L. P., and Lauretta D. S. 2005. Supernova olivine from cometary dust. *Science* 309:737–741.

Mostefaoui S. and Hoppe P. 2004. Discovery of abundant in situ silicate and spinel grains from red giant stars in a primitive meteorite. *The Astrophysical Journal* 613:L149–L152.

Nagashima K., Krot A. N., and Yurimoto H. 2004. Stardust silicates from primitive meteorites. *Nature* 428:921–924.

Nguyen A. N. 2005. Characterization of presolar silicate grains in primitive meteorites by multi-detection raster ion imaging in the NanoSIMS. Ph.D. thesis, Washington University, St. Louis, MO, 202 p.

Nguyen A. N. and Messenger S. 2014. Resolving the stellar sources of isotopically rare presolar silicate grains through Mg and Fe isotopic analyses. *The Astrophysical Journal* 784:1–15. doi:10.1088/0004-1637X/1784/1082/1149.

Nguyen A. N. and Zinner E. 2004. Discovery of ancient silicate stardust in a meteorite. *Science* 303:1496–1499.

Nguyen A. N., Stadermann F. J., Zinner E., Stroud R. M., Alexander C. M. O'D., and Nittler L. R. 2007. Characterization of presolar silicate and oxide grains in primitive carbonaceous chondrites. *The Astrophysical Journal* 656:1223–1240.

Nguyen A. N., Nittler L., Stadermann F. J., Stroud R., and Alexander C. M. O'D. 2010. Coordinated analyses of presolar grains in the Allan Hills 77307 and Queen Elizabeth Range 99177 meteorites. *The Astrophysical Journal* 719:166–189.

Nittler L. R. 2005. Constraints on heterogeneous galactic chemical evolution from meteoritic stardust. *The Astrophysical Journal* 618:281–296.

Nittler L. R., Alexander C. M. O'D., Gao X., Walker R. M., and Zinner E. 1997. Stellar sapphires: The properties and origins of presolar Al_2O_3 in meteorites. *The Astrophysical Journal* 483:475–495.

Nittler L. R., Alexander C. M. O'D., Gallino R., Hoppe P., Nguyen A. N., Stadermann F. J., and Zinner E. K. 2008. Aluminum-, calcium- and titanium-rich oxide stardust in ordinary chondrite meteorites. *The Astrophysical Journal* 682:1450–1478.

Ong W. J. and Floss C. 2013. Fe isotope nucleosynthesis: constraints from Fe isotopic analyses of presolar silicate grains from Acfer 094 (abstract #1163). 44th Lunar and Planetary Science Conference. CD-ROM.

Ong W. J., Floss C., and Gyngard F. 2012. Negative secondary ion measurements of $^{54}Fe/^{56}Fe$ and $^{57}Fe/^{56}Fe$ in presolar silicate grains from Acfer 094 (abstract #1225). 43rd Lunar and Planetary Science Conference. CD-ROM.

Rauscher T., Heger A., Hoffman R. D., and Woosley S. E. 2002. Nucleosynthesis in massive stars with improved nuclear and stellar physics. *The Astrophysical Journal* 576:323–348.

Stadermann F. J., Croat T. K., Bernatowicz T. J., Amari S., Messenger S., Walker R. M., and Zinner E. 2005. Supernova graphite in the NanoSIMS: Carbon, oxygen and titanium isotopic compositions of a spherule and its TiC sub-components. *Geochimica et Cosmochimica Acta* 69:177–188.

Stadermann F. J., Floss C., Bose M., and Lea A. S. 2009. The use of Auger spectroscopy for the in situ elemental characterization of sub-micrometer presolar grains. *Meteoritics & Planetary Science* 44:1033–1049.

Timmes F. X. and Clayton D. D. 1996. Galactic evolution of silicon isotopes: Application to presolar SiC grains from meteorites. *The Astrophysical Journal* 472:723–741.

Trappitsch R., Nittler L. R., Savina M. R., and Davis A. M. 2013. Modeling heterogeneous galactic chemical evolution for presolar grain comparison (abstract #5351). *Meteoritics & Planetary Science* 48:A314.

Van den Hoek L. B. and de Jong T. 1997. Inhomogeneous chemical evolution of the galactic disk: Evidence for sequential stellar enrichment. *Astronomy & Astrophysics* 318:231–251.

Vollmer C. and Hoppe P. 2010. First Fe isotopic measurement of a highly ^{17}O-enriched stardust silicate (abstract #1200). 41st Lunar and Planetary Science Conference. CD-ROM.

Vollmer C., Hoppe P., and Brenker F. E. 2008. Si isotopic compositions of presolar silicate grains from red giant stars and supernovae. *The Astrophysical Journal* 684:611–617.

Vollmer C., Hoppe P., Stadermann F. J., Floss C., and Brenker F. E. 2009. NanoSIMS analysis and auger electron microscopy of silicate and oxide stardust from the carbonaceous chondrite Acfer 094. *Geochimica et Cosmochimica Acta* 73:7127–7149.

Zinner E. 2013. Presolar grains. In *Meteorites and cosmochemical processes*, edited by Davis A. M. Treatise on Geochemistry, vol. 1.4, 2nd ed, edited by Holland H. D. and Turekian K. K. Oxford: Elsevier. pp. 181–213.

APPENDIX

Table A1. Oxygen isotopic compositions of presolar grains from Acfer 094.

Grain	Group	$^{17}O/^{16}O$ ($\times10^{-4}$)	$^{18}O/^{16}O$ ($\times10^{-3}$)	Phase
WU014-D				
02-02	4	8.08 ± 0.45	2.89 ± 0.08	n.m.
02-06	1	5.90 ± 0.34	1.76 ± 0.06	Fe, Al-silicate
02-07	1	7.31 ± 0.21	1.78 ± 0.03	Fe, Mg-silicate
04-01	4	3.89 ± 0.33	4.04 ± 0.10	Fe, Mg-silicate
04-03	4	3.97 ± 0.22	3.04 ± 0.06	Fe, Mg-silicate
05-01	1	4.91 ± 0.22	1.58 ± 0.04	Fe, Mg-silicate
06-06	1	5.86 ± 0.38	1.72 ± 0.06	Fe-silicate
06-07	1	5.83 ± 0.38	1.89 ± 0.07	Fe-silicate
06-08	1	5.44 ± 0.35	1.88 ± 0.06	Fe, Mg-silicate
07-01 (17)	1	6.66 ± 0.29	1.71 ± 0.05	Fe, Mg-silicate
07-01 (18)	1	3.97 ± 0.10	2.14 ± 0.02	Fe-silicate
09-04Lb	1	7.80 ± 0.37	2.28 ± 0.06	Fe-silicate
09-04Ra	1	5.53 ± 0.29	1.43 ± 0.05	Fe, Mg-silicate
10-06M	1	7.33 ± 0.28	1.78 ± 0.04	Fe, Mg-silicate
10-06T	1	13.5 ± 0.5	1.82 ± 0.05	Fe, Al-silicate
15-08	1	6.13 ± 0.42	1.84 ± 0.07	Fe-silicate
16-02	4	3.85 ± 0.20	2.12 ± 0.05	Fe, Mg-silicate
16-05	1	5.57 ± 0.20	1.54 ± 0.03	Fe, Mg-silicate
16-08	1	4.77 ± 0.26	1.85 ± 0.05	Fe-silicate
16-12	1	5.20 ± 0.22	1.88 ± 0.04	Fe-oxide
17-01	1	5.90 ± 0.21	1.72 ± 0.04	Fe-silicate
17-04	1	4.75 ± 0.22	1.60 ± 0.04	Fe-silicate
17-07	1	4.47 ± 0.17	1.66 ± 0.03	Fe, Mg-silicate
17-08	1	5.49 ± 0.20	1.78 ± 0.04	Fe, Mg-silicate
WU014-B				
01-05-01	1	4.68 ± 0.21	1.69 ± 0.04	Fe-oxide
02-01-01	1	4.44 ± 0.15	1.78 ± 0.03	Fe, Mg-silicate
02-01-02	1	4.53 ± 0.13	1.93 ± 0.03	Fe-silicate
02-01-03	1	4.36 ± 0.14	1.79 ± 0.03	Fe, Mg-silicate
02-01-04	1	4.29 ± 0.14	1.79 ± 0.03	Fe-silicate
02-07-01	1	3.95 ± 0.09	2.13 ± 0.02	Fe-silicate
02-07-02	1	9.22 ± 0.20	1.95 ± 0.03	Fe, Al-silicate
02-08-01	1	4.65 ± 0.15	1.55 ± 0.03	Fe, Mg, Al-silicate
03-04-01	4	3.56 ± 0.16	2.43 ± 0.04	Fe-silicate
03-05-01	1	4.26 ± 0.15	1.89 ± 0.03	n.m.
03-08-01	1	4.43 ± 0.20	1.90 ± 0.04	Fe, Al-silicate
03-11-01	1	4.38 ± 0.15	1.61 ± 0.03	Fe, Mg-silicate

Table A1. *Continued*. Oxygen isotopic compositions of presolar grains from Acfer 094.

Grain	Group	$^{17}O/^{16}O$ ($\times 10^{-4}$)	$^{18}O/^{16}O$ ($\times 10^{-3}$)	Phase
03-12-01	1	4.83 ± 0.15	1.87 ± 0.03	Fe, Mg, Al-silicate
03-13-01	1	4.32 ± 0.14	1.92 ± 0.03	Fe, Mg-silicate
05-01-01	1	27.0 ± 0.4	1.65 ± 0.03	Fe, Mg-silicate
08-04-01	1	4.72 ± 0.16	1.84 ± 0.03	Fe-silicate
08-05-01	1	5.39 ± 0.18	1.49 ± 0.03	Fe, Mg-silicate
09-03-01	1	4.92 ± 0.18	1.88 ± 0.03	Fe-silicate
09-06-01	1	6.53 ± 0.21	1.84 ± 0.04	Fe, Mg-silicate
09-06-03	4	3.49 ± 0.18	2.40 ± 0.05	n.m.
09-10-01	1	5.44 ± 0.16	1.57 ± 0.03	Fe, Mg-silicate
10-03-02	1	4.82 ± 0.17	1.92 ± 0.03	Fe, Mg-silicate
10-08-01	1	4.92 ± 0.21	1.79 ± 0.04	Fe-silicate
11-03-01	1	9.45 ± 0.27	1.80 ± 0.04	Fe-silicate
11-05-01	1	3.84 ± 0.14	2.09 ± 0.03	Fe-oxide
11-09-01	1	5.09 ± 0.17	1.80 ± 0.03	Fe, Mg-silicate
12-05-01	4	4.58 ± 0.12	2.30 ± 0.03	Fe-oxide
12-06-01	1	9.85 ± 0.38	1.73 ± 0.05	n.m.
12-06-02	1	5.00 ± 0.27	1.90 ± 0.05	n.m.
13-01-01	1	4.43 ± 0.18	1.68 ± 0.03	Fe-silicate
13-07-01	1	5.60 ± 0.27	1.92 ± 0.05	Fe-silicate
14-03-01	1	6.40 ± 0.27	1.35 ± 0.04	Fe-silicate
14-04-01	1	5.03 ± 0.19	1.89 ± 0.04	Fe, Mg-silicate
15-08-01	1	4.56 ± 0.17	1.94 ± 0.04	Fe-silicate
15-11-01	1	4.91 ± 0.22	1.57 ± 0.04	Fe-silicate
15-13-01	1	4.67 ± 0.20	1.91 ± 0.04	Fe, Mg-silicate
16-02-01	3	2.67 ± 0.13	1.79 ± 0.04	Fe, Mg-silicate
16-04-01	1	6.61 ± 0.36	1.72 ± 0.06	Fe, Mg-silicate
17-05-02	1	5.49 ± 0.21	1.74 ± 0.04	n.m.
17-06-01	1	9.09 ± 0.28	1.77 ± 0.04	Fe-silicate
17-07-01	1	5.31 ± 0.19	1.76 ± 0.03	n.m.
17-09-01	4	5.16 ± 0.19	2.31 ± 0.04	n.m.
18-01-02	1	10.1 ± 0.3	1.78 ± 0.04	Fe, Mg-silicate
18-01-03	1	4.46 ± 0.17	1.90 ± 0.04	Fe-silicate
18-02-01	1	8.23 ± 0.25	1.82 ± 0.04	Fe, Mg-silicate
19-01-01	1	4.70 ± 0.20	1.82 ± 0.04	n.m.
19-01-02	1	4.50 ± 0.18	1.88 ± 0.04	n.m.
19-05-01	1	4.55 ± 0.19	1.93 ± 0.04	n.m.
19-05-02	3	3.08 ± 0.16	1.61 ± 0.04	n.m.
19-07-01	1	6.38 ± 0.28	1.78 ± 0.05	Fe-silicate
19-10-02	1	4.55 ± 0.19	1.72 ± 0.04	Fe, Mg-silicate
WU029-3				
03-04(1)	4	2.60 ± 0.46	2.60 ± 0.14	Fe-silicate
03-04(2)	1	6.19 ± 0.60	1.98 ± 0.10	Fe, Al-oxide
05-01	1	10.4 ± 0.9	1.71 ± 0.10	Fe, Mg-silicate
05-04	1	17.2 ± 0.6	1.77 ± 0.06	Fe-silicate
06-03	1	5.58 ± 0.41	1.87 ± 0.06	Fe, Mg-silicate
08-03	1	6.07 ± 0.72	1.63 ± 0.11	n.m.
09-04	1	5.92 ± 0.66	1.88 ± 0.11	Fe-silicate
WU029-4				
12-03	1	6.86 ± 0.72	1.54 ± 0.11	Fe, Mg, Al-silicate
14-03	1	9.70 ± 0.35	1.79 ± 0.05	Fe, Mg-silicate
15-02	1	5.11 ± 0.23	1.93 ± 0.04	Fe, Mg, Al-silicate
16-03	1	7.76 ± 0.35	1.92 ± 0.05	Fe, Mg-silicate
16-06	1	6.63 ± 0.35	1.80 ± 0.06	Fe, Mg-silicate
17-06	4	3.10 ± 0.21	2.20 ± 0.05	Fe-silicate

Table A1. *Continued*. Oxygen isotopic compositions of presolar grains from Acfer 094.

Grain	Group	$^{17}O/^{16}O$ ($\times 10^{-4}$)	$^{18}O/^{16}O$ ($\times 10^{-3}$)	Phase
19-05	1	7.12 ± 0.33	1.53 ± 0.05	Fe, Mg-silicate
20-03	1	6.08 ± 0.35	1.42 ± 0.05	Fe-silicate
20-06	1	5.58 ± 0.35	1.78 ± 0.06	Fe, Mg-silicate
22-03	1	6.29 ± 0.53	1.72 ± 0.08	Fe-oxide
22-08	1	5.09 ± 0.35	1.45 ± 0.06	Fe-silicate
22-09	1	7.19 ± 0.35	1.77 ± 0.05	Fe-silicate